JOURNAL OF APPLIED PHYSICS **108**, 023711 (2010)

Scanning tunneling spectroscopy and Kelvin probe force microscopy investigation of Fermi energy level pinning mechanism on InAs and InGaAs clean surfaces

Wilhelm Melitz,[1,2] Jian Shen,[1,2] Sangyeob Lee,[2] Joon Sung Lee,[1,2] Andrew C. Kummel,[2,a)] Ravi Droopad,[3] and Edward T. Yu[4]
[1]*Materials Science and Engineering Program, University of California, San Diego, La Jolla, California 92093, USA*
[2]*Department of Chemistry and Biochemistry, University of California, San Diego, La Jolla, California 92093, USA*
[3]*Department of Physics, Texas State University, San Marcos, Texas 78666, USA*
[4]*Department of Electrical and Computer Engineering, The University of Texas at Austin, Austin, Texas 78758, USA*

(Received 27 April 2010; accepted 11 June 2010; published online 29 July 2010)

A comparison is made between the electronic structures determined in ultrahigh vacuum of three surfaces using scanning tunneling spectroscopy (STS) and Kelvin probe force microscopy (KPFM). STS and KPFM illustrates Fermi level pinning of clean InAs(001)-(4 × 2) and InGaAs(001)-(4 × 2) surfaces and near flat band conditions for InAs(110) cleaved surfaces. However, for InAs(001)-(4 × 2) and InGaAs(001)-(4 × 2), STS and KPFM data show very different positions for the surface Fermi level on identical samples; it is hypothesized that the difference is due to the Fermi level measured by KPFM being shifted by a static charge dipole to which STS is much less sensitive. © *2010 American Institute of Physics*. [doi:10.1063/1.3462440]

I. INTRODUCTION

InAs and InGaAs have shown great promise as channel materials for metal oxide semiconductor field effect transistors (MOSFETs) because of extremely high electron mobility.[1] One limiting factor for the development of III–V MOSFETs is the oxide/semiconductor interface quality. For growth of MOSFET gate oxides, atomic layer deposition (ALD) is employed to deposit gate oxides on the semiconductor by exposure to metal organic and oxidant gases. The goal of ALD is for the oxidants to selectively oxidize the metal precursor chemisorbates without oxidizing the substrate. A reconstruction of InAs(001) or InGaAs(001) with low reactivity to oxidants, such as the In-rich (4 × 2) surface reconstruction[2–4] is desirable to minimize substrate oxidation that can introduce surface states and degrade device performance.

Ultrahigh vacuum (UHV)-cleaved InAs(110) surfaces only contain In–As bonds with a similar structure to the cleaved GaAs surface.[5] For InAs(110), an idealized model of the surface has the surface atoms buckling into geometries which are relaxed with the particular dangling bonds on each type of atom: the As atoms have a sp^3 hybridized bonding geometry with a completely filled dangling bond while the In atoms have sp^2 hybridized bonding geometry with a completely empty dangling bond. The InAs(110) surface being unpinned is consistent with having completely filled and empty dangling bonds in a relaxed geometrical structure with low defect density and no partially filled dangling bonds. The InGaAs(110) surface is not studied here because InGaAs thin films are grown on other compound semiconductor wafers making it more challenging to perform cross-sectional studies.

The surface structure of InAs(001)-(4 × 2) has been studied using scanning tunneling microscopy (STM),[3,6–8] reflection high-energy electron diffraction (RHEED),[7] and density functional theory (DFT).[3,6,9] The InAs(001)-(4 × 2) surface contains dicoordinated In row atoms and pairs of In homodimers in the trough. The tricoordinated In and As atoms normally have completely filled or empty dangling bonds. The homodimers or row dicoordinated In atoms on the InAs(001)-(4 × 2) surface could generate surface states, causing surface pinning. The InAs(001)-(4 × 2) surface shows electron accumulation and a surface dipole, caused by surface states. The InGaAs(001)-(4 × 2) surface structure is analogous to InAs(001)-(4 × 2), with some In atoms replaced with Ga atoms. The InGaAs(001)-(4 × 2) surface structure has also been studied with STM,[4,10] RHEED,[10] and DFT.[4,11,12]

A combination of Kelvin probe force microscopy (KPFM) (Refs. 13 and 14) and scanning tunneling spectroscopy (STS) (Refs. 15–19) is used here to illustrate the pinning of clean InAs(001)-(4 × 2) and InGaAs(001)-(4 × 2) surfaces and unpinning of InAs(110) cleaved surfaces. In a comparison of STS and KPFM data, both show that the Fermi level of InAs(110) is unpinned. However, for InAs(001)-(4 × 2) and InGaAs(001)-(4 × 2), STS and KPFM show very different positions for the Fermi level on identical samples, which is hypothesized to occur because the Fermi level is shifted by a static surface charge dipole to which KPFM is sensitive but STS is not.

[a)] Electronic mail: akummel@ucsd.edu.

II. EXPERIMENTAL TECHNIQUE

The InAs samples are commercially available InAs wafers (Wafer Tech) with a 200 nm thick InAs surface layer grown by molecular beam epitaxy (MBE). The *n*-type and *p*-type InAs substrates have 2×10^{18} cm^{-3} doping with S and Zn dopants. The *n*-type and *p*-type MBE-grown InAs layers have 2×10^{18} cm^{-3} doping with Si and Be dopants. The InGaAs samples consist of commercially available InP wafers with a 0.2 μm thick $In_{0.53}Ga_{0.47}As$ surface layer grown by MBE. The InP substrate dopings for both *n*-type and *p*-type InAs are 2×10^{18} cm^{-3} with Si and Zn dopants. The MBE-grown InGaAs layers are doped *n*-type and *p*-type 2×10^{18} cm^{-3} with Si and Be dopants.

Following MBE growth, all samples are capped with a 50 nm As_2 layer and shipped/stored under vacuum before loading into the UHV chamber. Sample preparation is performed in a preparation chamber with a base pressure of mid 10^{-10} Torr. The samples are first degassed at 150 °C followed by a two hour As_2 layer decapping at ~330 °C. After decapping, the samples are annealed at 450–470 °C to form the InAs(001)-(4×2) or InGaAs(001)-(4×2) surface reconstruction. For InAs(110), samples are degassed at 150 °C for several hours before cleaving in UHV.

An Omicron VT-AFM/STM analysis chamber, with a base pressure in the low 10^{-11} Torr, is used for STM/STS and KPFM. An etched W wire is cracked in UHV and employed for STM/STS. STS can be performed with constant tip sample distance or with variable tip distance.[18–22] Variable tip STS is employed with z variation of 0.1–0.3 nm/V and tip sample distances of 0.2–0.5 nm. KPFM was performed with commercial Pt coated silicon cantilevers from Asylum Research. Frequency modulation (FM) (Ref. 23) and amplitude modulation (AM) (Ref. 24) KPFM are performed with cantilevers with resonant frequencies of approximately 270 kHz and 70 kHz, respectively.

KPFM measures the contact potential difference (CPD) between the sample and tip. The CPD is defined as

$$\mathrm{CPD} = \varphi_{\mathrm{tip}} - \varphi_{\mathrm{sample}}, \tag{1}$$

where φ_{tip} is the work function of the metallic tip and $\varphi_{\mathrm{sample}}$ is the work function of the sample surface. The work function of Pt-coated tips is first calibrated with highly ordered pyrolytic graphite (HOPG) ($\varphi_{\mathrm{HOPG}}=4.6\pm0.1$ eV) (Ref. 25) to convert the measured CPD to the absolute surface work function. The absolute surface work function of the sample can be calculated as follows

$$\varphi_{\mathrm{sample}} = 4.6\ \mathrm{eV} + \mathrm{CPD}_{\mathrm{HOPG}} - \mathrm{CPD}_{\mathrm{sample}}. \tag{2}$$

To determine an absolute work function with a scanning KPFM, a scan over a large area is taken, and the mean of the distribution of CPD at each point is employed as the sample CPD. A Pt coated silicon cantilever is used at a frequency set point of −50 Hz relative to the resonant frequency of the cantilever, corresponding to a typical tip sample separation of approximately 3 nm. A scan of larger then 100 $\times100$ nm^2 is performed on both the sample and HOPG to determine $\mathrm{CPD}_{\mathrm{sample}}$ and $\mathrm{CPD}_{\mathrm{HOPG}}$.

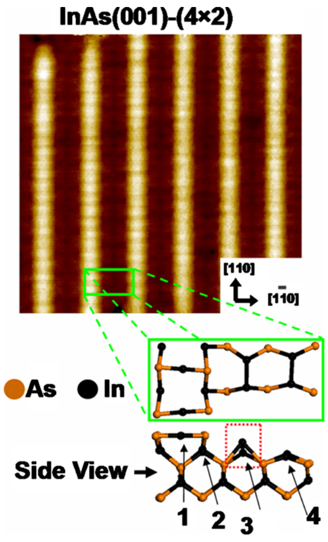

FIG. 1. (Color online) (a) High resolution filled state STM of InAs(001)-(4×2) and ball-stick diagram of surface reconstruction. Scan size is 11×11 nm^2.

III. RESULTS

A. STM

Figure 1 shows a high resolution STM image of an InAs(001)-(4×2) surface, with a unit cell indicated by the green rectangle. The STM image contains a row and trough structure consistent with the $\beta3'(4\times2)$ (Ref. 6) reconstruction containing two row dicoordinated In atoms (arrow 1), four row tricoordinated edge As atoms (arrow 2) and two tricoordinated In homodimers located in the trough (arrows 3 and 4). In contrast to the InAs(110) surface, the InAs(001)-(4×2) surface reconstruction may have several potential defect sites including partially filled dangling bonds which introduce defects that can cause Fermi energy level pinning.[26]

The InGaAs(001)-(4×2) surface structure is similar to InAs(001)-(4×2) with more surface defects. The structure is identical with some of the surface In atoms replaced with Ga atoms. Figure 2(a) shows a typical InGaAs(001)-(4×2) surface. Figure 2(b) illustrates a typical InAs(001)-(4×2) surface with the same length scale. Four kinds of defects are typically observed on InGaAs(001)-(4×2). The first is dark cuts in the rows [inset of Fig. 2(a)]. The second is bright dots above the trough or the row [inset of Fig. 2(b)]. The third is dark rows perpendicular to the In rows, [the rectangle in Fig. 2(a)]. The fourth is bright rows parallel to the In rows [the oval in Fig. 2(b)]. Figure 2 shows InGaAs(001)-(4×2) consistently has more defects than InAs(001)-(4×2).[12]

High resolution STM of a cleaved InAs(110) surface is shown in Fig. 3. The periodic structure matches the bulk lattice spacing of 0.6×0.4 nm^2.[5,27] The InAs(110) cross-sectional surface only contains heterogeneous In–As bonds and is atomically flat with few defects which would contribute defect states.[5] The As atoms are oriented in a sp^3 hybridized bonding configuration with a filled dangling bond in a simplified model. The In atoms are oriented in a sp^2 hybridized bonding configuration with an empty dangling bond in a simplified model. Only the As atoms appear in the high res-

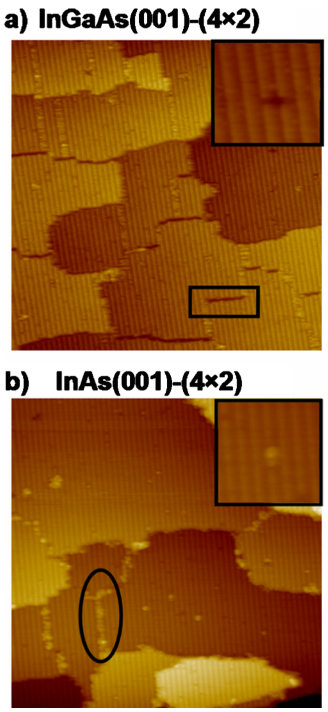

FIG. 2. (Color online) (a) 100×100 nm^2 filled state STM of typical InGaAs(001) surface. (b) 100×100 nm^2 filled state STM of typical InAs(001) surface.

olution filled state STM because the surface As atoms have filled dangling bonds while surface In atoms have empty dangling bonds. The structure of InAs(110) is analogous to that of the GaAs(110).[20,28]

B. STS

STS spectra were collected for both *n*-type and *p*-type InAs(001)-(4×2). With no tip-induced band bending, zero sample bias corresponds approximately to the location of the surface Fermi level relative to the conduction band minimum (CBM) and the valence band maximum (VBM).[20,29] As shown in Fig. 4(a), both *n*-type and *p*-type InAs(001)-(4×2) have zero sample bias near the CBM, consistent with the surface Fermi level being pinned *n*-type. For an unpinned surface, the Fermi level position, at zero bias, for *n*-type and *p*-type should have a shift relative to the VBM and CBM. Furthermore, the surface Fermi level for InAs(001)-(4×2) is known to be pinned at the CBM from ultraviolet photoelectron spectroscopy (UPS) and high resolution electron energy loss spectroscopy[30,31] experiments. The STS for InAs(001)-(4×2) shows a band gap of 0.3 eV, close to the expected band gap of 0.35 eV and consistent with minimal tip-induced band bending. If the surface Fermi level is pinned, the amount of tip-induced band bending will be minimal, because surface states can be filled or empty to account for the work function difference between the W tip and the InAs(001)-(4×2) surface.[32,33]

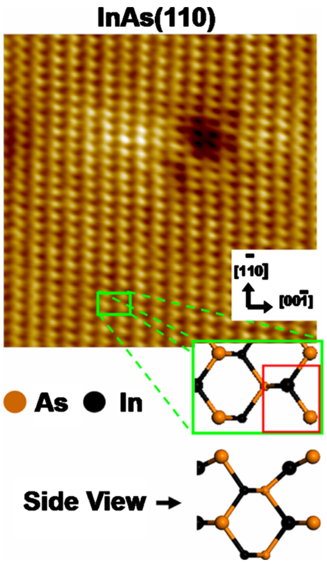

FIG. 3. (Color online) High resolution filled state STM of InAs(001) surface and ball and stick diagram of surface. Scan size is 11×11 nm^2.

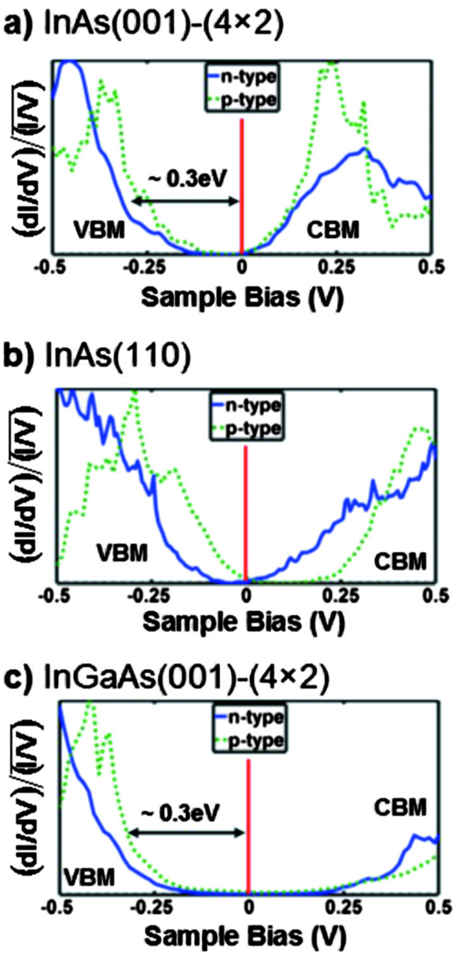

FIG. 4. (Color online) Normalized $(dI/dV)/(\overline{I/V})$ spectra of (a) InAs(001)-(4×2), (b) cleaved InAs(110), and (c) InGaAs(001)-(4×2) using variable-*z* STS. Δz for spectra ranges from 0.1–0.3 nm/V. I/V is smoothed before $(dI/dV)/(\overline{I/V})$ is calculated (Ref. 17).

The InAs(110) surface contains only filled or empty dangling bonds on tricoordinated atoms in relaxed geometries which should be electrically passive.[26] Therefore, the surface is expected to be unpinned. The STS [Fig. 4(b)] image of InAs(110) in cross-section shows the Fermi level for *n*-type InAs(110) near the CBM and the Fermi level for *p*-type InAs(110) close to the VBM. The shift between *n*-type and *p*-type is about 0.2 eV, consistent with an unpinned InAs surface. The STS for InAs(110) shows a band gap of around 0.2 eV, however, the band gap of InAs is 0.35 eV. The decrease in band gap is caused by the variable *z* spectroscopy used for the STS. When doing variable *z*, enhancement of the signal can occur on unpinned surfaces for low sample biases causing a smearing effect on the valence band (VB) and conduction band (CB).[20] Tip-induced band bending should be minimal for InAs(110) because of the high doping level and the small band gap of the InAs sample. The high doping will reduce the space charge region formed by the CPD of the W tip and the semiconductor. The small band gap will also provide a large density of states (DOS) that will respond to the potential difference again reducing the amount of tip-induced band bending.[32–34]

STS on InGaAs(001)-(4 × 2) has an advantage over STS on InAs(001)-(4 × 2), because the band gap of InGaAs is 0.74 eV (compared to InAs of 0.35 eV), which produces more consistent spectra. InGaAs(001)-(4 × 2) is expected to have similar electronic properties to InAs(001)-(4 × 2) because the surface reconstructions are effectively the same except the group III atoms on InGaAs(001)-(4 × 2) surfaces are a weighted random mixture of In and Ga atoms. However, in Fig. 4(c), the Fermi level (zero bias position) as determined by STS is located near the VBM or midgap for both *n*-type and *p*-type, consistent with InGaAs(001)-(4 × 2) being pinned *p*-type or midgap. Note that the position of the zero bias relative to the VBM for both InGaAs(001)-(4 × 2) and InAs(001)-(4 × 2) is approximately the same, 0.3 eV above the VBM. The VB offset for InGaAs and InAs of ~0.1 eV (Ref. 35) which positions the Fermi level measure with STS for both InGaAs(001)-(4 × 2) and InAs(001)-(4 × 2) at the same position within 0.1 eV. The STS indicates the surface Fermi level positions of InGaAs and InAs (4 × 2) surfaces are roughly at the same energy relative to the VB. A wide range of positions for the surface Fermi level of InGaAs(001) have been reported. As explained below, UPS measurements of the Fermi level position should be consistent with STS measurements of the Fermi level position. To our knowledge, no UPS results on decapped MBE-grown InGaAs/InP have been published. UPS results on metal-organic vapor phase epitaxy (MOVPE) InGaAs/InP show the surface Fermi level ~0.4 eV above the VBM.[36] Photoluminescence (PL) spectroscopy and metal insulator semiconductor structures on InGaAs indicated the position of the surface Fermi level is ~0.5 eV above the VBM.[37,38] However, these studies did not document the reconstruction or the UHV cleaning method so the difference in Fermi level position between the previous studies and the present one may be due to differences in the reconstruction or UHV preparation.

C. KPFM

The KPFM results for both the InAs(001)-(4 × 2) and the InAs(110) surfaces are shown in Fig. 5. The KPFM data is consistent with the STS results showing the InAs(001)-(4 × 2) surface reconstruction is pinned and the InAs(110) surface is unpinned. KPFM shows the pinned surface InAs(001)-(4 × 2) work function is much lower than the expected value from bulk properties, consistent with an electron accumulation layer and/or dipole on the surface.

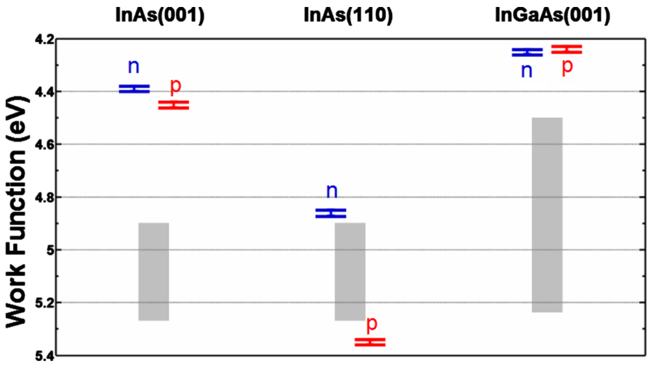

FIG. 5. (Color online) KPFM measured work functions from AM mode measurement along with bulk band gaps. The *n*-type (n) and *p*-type (p) work functions are measured on separate samples. The rectangles indicate the band gap energies calculated from the bulk electron affinities and band gaps. Left: InAs(001) surfaces have *n*-type and *p*-type surface work functions pinned in the CB. Middle: InAs(110) surfaces have unpinned bulk-like work functions. Right: InGaAs(001) surfaces have *n*-type and *p*-type surface work functions pinned in the CB.

Figure 5 (left) shows AM mode KPFM for both the *n*-type and *p*-type InAs(001)-(4 × 2) surfaces. The measured surface work functions of *n*-type and *p*-type InAs(001)-(4 × 2) are 4.39 ± 0.01 eV and 4.43 ± 0.01 eV, respectively, with a cantilever calibration error of ±0.1 eV. The cantilever calibration error arises from the uncertainty of the absolute work function of HOPG. The electron affinity of InAs is 4.9 eV, which puts the surface work function of *n*-type and *p*-type InAs(001)-(4 × 2), 0.51 eV and 0.47 eV, respectively, above the CBM. AM mode KPFM shows consistent results with a standard deviation of 0.016 eV and a full width half maximum less than 0.011 eV over several samples. FM mode KPFM on *n*-type and *p*-type InAs(001)-(4 × 2) surfaces shows work functions of 4.30 ± 0.1 eV and 4.34 ± 0.1 eV, respectively. The KPFM measurements are consistent with the InAs(001)-(4 × 2) surface reconstruction being pinned deep in the CB, in accordance with an electron accumulation and/or surface dipole.

Figure 5 (middle) shows both the AM mode KPFM for *n*-type and *p*-type InAs(110) cross-section surfaces. The KPFM results on the InAs(110) cross-sectional surface agrees with the STS results, showing work functions of *n*-type and *p*-type near the theoretical bulk values. The measured surface work functions of *n*-type and *p*-type InAs(110) are 4.84 ± 0.01 eV and 5.35 ± 0.01 eV, respectively, with a cantilever calibration error of ±0.1 eV. The bulk Fermi energy level position for *n*-type InAs is approximately 0.5 eV above the VBM for a doping density of 1×10^{18} cm^{-3}.[39,40] The bulk Fermi level *p*-type InAs for doping concentration of 1×10^{17} cm^{-3} is 0.09 eV above the VBM.[40] If the bulk work functions are measured for *n*-type and *p*-type, a difference of 0.41 eV should be observed. KPFM shows a 0.51 ± 0.2 eV difference. The measured difference of *n*-type and *p*-type is consistent with flat band conditions.[18] AM mode KPFM showed consistent results, with a standard deviation of 0.011 eV, and a full width half maximum less than 0.015 eV over several samples. FM mode KPFM is also performed with *n*-type and *p*-type InAs(110) cross-sectional surfaces having a surface work functions of 4.83 ± 0.1 eV and 5.31 ± 0.1 eV, respectively. KPFM on the InAs(110) cross-sectional surface demonstrates that the surface Fermi energy level is unpinned.

Figure 5 (right) shows AM mode KPFM for both the *n*-type and *p*-type InGaAs(001)-(4 × 2). The surface work functions of *n*-type and *p*-type are 4.25 ± 0.01 eV and 4.24 ± 0.01 eV, respectively, with a cantilever calibration error of ±0.1 eV. AM mode KPFM showed consistent results with a standard deviation of 0.056 eV and a full width half maximum less then 0.011 eV over several samples. FM mode KPFM shows *n*-type and *p*-type InGaAs(001)-(4 × 2) surfaces having work functions of 4.1 ± 0.1 eV and 4.1 ± 0.1 eV. The electron affinity of InGaAs is 4.5 eV, and the KPFM data would therefore suggest that the surface Fermi level of *n*-type and *p*-type InGaAs(001)-(4 × 2) is 0.25 eV and 0.26 eV above the CB edge. KPFM shows the InGaAs(001)-(4 × 2) a smaller work function than expected surface, indicating an electron accumulation and/or surface dipole.[37,38] As discussed below, however, we postulate that this difference arises from the presence of a surface dipole that shifts the surface Fermi level measured by KPFM relative to that measured by other techniques such as STS or photoemission.

IV. DISCUSSION

STS and KPFM of the InAs(001)-(4 × 2) surfaces show one notable difference. For STS on InAs(001)-(4 × 2), the surface Fermi energy level appears in the band gap near the CBM, while KPFM shows the surface work function deep into the CB. It is proposed that the difference of the surface Fermi level between STS and KPFM is due to an intrinsic difference in the two methods. KPFM is extremely sensitive to fixed charges and surface dipoles, while it is proposed that the band-edge energies and surface Fermi level positions measured by STS are much less sensitive to fixed surface charge. STS measures the dynamic tunneling conductance which is proportional to the surface DOS,[19,41]

$$(dI/dV)/\overline{(I/V)} \propto \mathrm{DOS}_{\mathrm{sample}}(E_F - eV). \tag{3}$$

Figure 6(a) and 6(b) shows the band bending due to the surface states, indicated in the orange region, along with the effective surface work function caused by the surface dipole, indicated by red region. Figure 6(a) illustrates the different tunneling mechanisms in STS for InAs(001)-(4 × 2) in the presence of a static charge layer located on the surface. The solid arrow indicates the conditions under positive sample bias where the tunneling current is dominated by electrons from the tip to empty CB states, ignoring the static charge layer. The dashed arrow points to the conditions under negative sample bias where the tunneling is dominated by electrons from the sample's VB to the tip,[5,21,42] again ignoring the static charge layer. The static charge might influence the absolute tip sample distance in STS, which will have a slight but negligible, effect on the measured tunneling. For STS to ignore the states charge the static charge would need to be located physically closer to the tip than the surface states responsible for the pinning of the surface Fermi level.

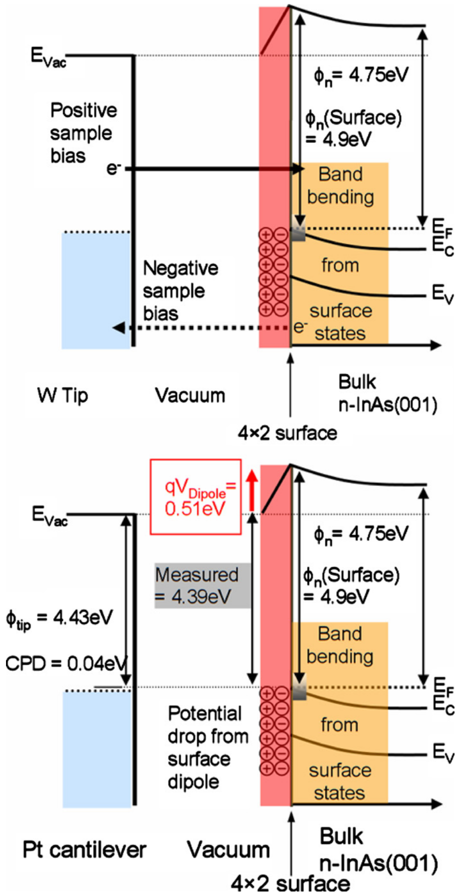

FIG. 6. (Color online) (a) Band diagram illustrating the dominate tunneling mechanisms during STS on *n*-InAs(001). The presence of a surface dipole is of little effect to the tunneling conditions. The position of the surface Fermi level is pinned near the CBM caused by surface states. (b) Band diagram illustrating the effects of a surface dipole has large effect upon the CPD of *n*-type InAs(001) measured with KPFM.

If the static charge or surface dipole is a thin layer above the surface states it is possible to have little or no influence on the amount of band bending in the semiconductor, because the surface states have already pinned the Fermi level. Optical based techniques measure the amount of band bending at the surface relative to the bulk, therefore optical based techniques would also not observe the presence of a static charge layer. UPS on InAs(001)-(4 × 2) shows the surface Fermi level 0.3–0.5 eV above the VBM.[30,43] The difference in Fermi level position is dependent on the surface preparation method. Samples prepared with ion-bombardment and annealing, show surface Fermi level 0.5 eV above the VBM, while decapped InAs is located 0.3 eV above the VBM.[44,45] The InAs(001)-(4 × 2) samples used in this paper are decapped MBE-grown wafers so the surface Fermi level near the CBM is expected. No significant difference in the position of the surface Fermi level between UPS and STS is observed. Both UPS and STS consistently show both *n*-type and *p*-type InAs(001)-(4 × 2) are pinned near or in the CB. However, an estimated difference in the position of surface Fermi level between UPS/STS and KFPM is 0.4–0.51 eV for InAs(001)-(4 × 2).

The main differences between STS and KPFM are the interactions with fixed surface charge or surface dipole. Figure 6(b) shows a band diagram illustrating a potential drop across a surface dipole influencing the measured surface work function of n-type InAs(001)-(4×2) with KPFM. Two potential features might cause a surface dipole: surface defects or strained surface atoms. Defects, like step edges or dislocations, can be traps sites exhibiting long time constants, acting as fixed charges. The InAs(001)-(4×2) surface has strained atoms or a strained reconstruction[12] producing charge transfers from bulk atoms to the surface atoms, and potentially causing fixed surface dipoles. A small amount of charge transfer can cause a significant potential drop at the surface. To simplify, the charge transfer is assumed to be perfectly perpendicular to the surface and spread over one atomic layer. The density of trapped charge on the surface required to account for a 0.4–0.51 eV potential difference between STS and KPFM is estimated with the following equation:

$$V_{\mathrm{dipole}} = \frac{qQ_{\mathrm{fixed}}\Delta qr}{\varepsilon_0}, \tag{4}$$

where ε_0 is the vacuum permittivity, r is the one atomic layer (~ 3 Å), and Δq is the charge transfer per defect (assumed to be one). A density of fixed charge of $Q_{\mathrm{fixed}} \approx 7.3-9.3 \times 10^{12}$ cm^{-2} could generate a dipole voltage drop of 0.4–0.51 eV.

The existence of surface states and fixed charges on InAs(001)-(4×2) is further supported by comparing the STS and KPFM results to the InAs(110) surface, known to be unpinned, with a low defect density. Cleaved InAs(110) has flat band conditions.[5,18] The work functions of the InAs(110) cross-sectional surfaces measured with KPFM are 4.84 ± 0.1 eV and 5.35 ± 0.1 eV for n-type and p-type. A difference of 0.2 ± 0.4 eV is estimated for STS and KPFM on n-type InAs(110). The STS error can be as high as ± 0.3 eV.[41] With few surface states, STS will be extremely sensitive to any potential difference between the tip and the surface and is more susceptible to tip-induced band bending.[32–34] For p-type, the difference between the two measurements for both STS and KPFM is within the measurement error. The STS and KPFM results for the InAs(110) cross-sectional surface indicate the expected results for an InAs surface having low defect density and low static charge density.

The density of surface defects also influences the static charge. The defect densities on InGaAs(001)-(4×2) are higher than InAs(001)-(4×2). STS for both InGaAs(001)-(4×2) and InAs(001)-(4×2) show the surface Fermi level approximately 0.3 eV above the VBM. The STS results for InGaAs(001)-(4×2) are consistent with the Fermi level position measured with UPS and PL showing the surface Fermi level in the band gap. The estimated difference in the position of surface Fermi level between PL/UPS/STS and KFPM for InGaAs(001)-(4×2) is 0.4–0.69 eV, corresponding to a fixed charge density of $Q_{\mathrm{fixed}} \approx 7.3-12 \times 10^{12}$ cm^{-2}. The fixed charge is likely to be caused by a combination of the strained surface reconstruction and the surface defects.

V. SUMMARY

STS and KPFM was performed on InAs(001)-(4×2), InAs(110), and InGaAs(001)-(4×2). STS shows InAs(001)-(4×2) and InGaAs(001)-(4×2) are pinned 0.3 eV above the VBM while InAs(110) is consistent with flat band conditions. The KPFM results are consistent with the InAs(110) STS results. The measured CPD for InAs(001)-(4×2) and InGaAs(001)-(4×2) indicates the presence of static charge. It is proposed that the discrepancy between STS and KPFM is due the differential influence of static charges or surface dipoles on these techniques. It is proposed that STS ignores any static charge because the measurement observes only current flow into/from partially filled states. Conversely, KPFM is highly sensitive to static charge because KPFM minimizes the electrostatic forces between the surface and the tip. By combining STS and KPFM to probe clean surfaces, the surface states and the static charges can be measured for surfaces with a large number of static charges.

ACKNOWLEDGMENTS

This work was supported by NSF under Grant Nos. NSF-DMR-0706243, Intel, SRC-NCRC-1437.003, and FCRP-MSD-887.011.

[1] N. Li, E. S. Harmon, J. Hyland, D. B. Salzman, T. P. Ma, Y. Xuan, and P. D. Ye, Appl. Phys. Lett. **92**, 143507 (2008).
[2] C. Ratsch, W. Barvosa-Carter, F. Grosse, J. H. G. Owen, and J. J. Zinck, Phys. Rev. B **62**, R7719 (2000).
[3] J. B. Clemens, S. R. Bishop, D. L. Feldwinn, R. Droopad, and A. C. Kummel, Surf. Sci. **603**, 2230 (2009).
[4] J. Shen, D. L. Winn, W. Melitz, J. B. Clemens, and A. C. Kummel, ECS Trans. **16**, 463 (2008).
[5] E. T. Yu, Chem. Rev. **97**, 1017 (1997).
[6] D. L. Feldwinn, J. B. Clemens, J. Shen, S. R. Bishop, T. J. Grassman, A. C. Kummel, R. Droopad, and M. Passlack, Surf. Sci. **603**, 3321 (2009).
[7] H. Yamaguchi and Y. Horikoshi, Phys. Rev. B **51**, 9836 (1995).
[8] C. Kendrick, G. LeLay, and A. Kahn, Phys. Rev. B **54**, 17877 (1996).
[9] R. H. Miwa, R. Miotto, and A. C. Ferraz, Surf. Sci. **542**, 101 (2003).
[10] H. Wen, Z. Wang, and G. J. Salamo, *Two-Dimensional Epitaxial Growth of Strained InGaAs on GaAs(001)*, MRS Symposia Proceedings No. 737, F3.19.1 (Materials Research Society, Pittsburgh, 2002).
[11] A. Chakrabarti, P. Kratzer, and M. Scheffler, Phys. Rev. B **74**, 245328 (2006).
[12] J. Shen, J. B. Clemens, E. A. Chagarov, D. L. Feldwinn, W. Melitz, T. Song, S. R. Bishop, R. Droopan, and A. C. Kummel, "Structural and electronic properties of group III rich $In_{0.53}Ga_{0.47}As(001)$," Surf. Sci. (in press).
[13] M. Nonnenmacher, M. P. Oboyle, and H. K. Wickramasinghe, Appl. Phys. Lett. **58**, 2921 (1991).
[14] T. R. Albrecht, P. Grutter, D. Horne, and D. Rugar, J. Appl. Phys. **69**, 668 (1991).
[15] R. M. Feenstra, Surf. Sci. **299–300**, 965 (1994).
[16] J.A. Stroscio, R.M. Feenstra, D.M. Newns, and A.P. Fein, J. Vac. Sci. Technol. A **6**, 499 (1988).
[17] P. Mårtensson and R. M. Feenstra, Phys. Rev. B **39**, 7744 (1989).
[18] W. Mönch, *Semiconductor Surfaces and Interfaces* (Springer-Verlag, Berlin, New York, 1995).
[19] R. J. Hamers and D. F. Padowitz, *Scanning Probe Microscopy and Spectroscopy: Theory, Techniques, and Applications*, 2nd ed. (Wiley, New York, 2001).
[20] J. A. Stroscio and W. J. Kaiser, *Scanning Tunneling Microscopy* (Academic, Boston, 1993).
[21] N. D. Jager, E. R. Weber, K. Urban, and P. Ebert, Phys. Rev. B **67**, 165327 (2003).
[22] S. Landrock, Y. Jiang, K. H. Wu, E. G. Wang, K. Urban, and P. Ebert, Appl. Phys. Lett. **95**, 072107 (2009).

[23] S. Kitamura and M. Iwatsuki, Appl. Phys. Lett. **72**, 3154 (1998).

[24] A. Kikukawa, S. Hosaka, and R. Imura, Appl. Phys. Lett. **66**, 3510 (1995).

[25] M. M. Beerbom, B. Lagel, A. J. Cascio, B. V. Doran, and R. Schlaf, J. Electron Spectrosc. Relat. Phenom. **152**, 12 (2006).

[26] S. G. Davison and M. Stęślicka, *Basic Theory of Surface States* (Clarendon/Oxford University Press, Oxford/New York, 1992).

[27] A. Schwarz, W. Allers, U. D. Schwarz, and R. Wiesendanger, Phys. Rev. B **61**, 2837 (2000).

[28] R. M. Feenstra, J. A. Stroscio, J. Tersoff, and A. P. Fein, Phys. Rev. Lett. **58**, 1192 (1987).

[29] H. Hasegawa, N. Negoro, S. Kasai, Y. Ishikawa, and H. Fujikuwa, J. Vac. Sci. Technol. B **18**, 2100 (2000).

[30] M. Noguchi, K. Hirakawa, and T. Ikoma, Phys. Rev. Lett. **66**, 2243 (1991).

[31] L. O. Olsson, C. B. M. Andersson, M. C. Hakansson, J. Kanski, L. Ilver, and U. O. Karlsson, Phys. Rev. Lett. **76**, 3626 (1996).

[32] R. M. Feenstra, Y. Dong, M. P. Semtsiv, and W. T. Masselink, Nanotechnology **18**, 044015 (2007).

[33] M. McEllistrem, G. Haase, D. Chen, and R. J. Hamers, Phys. Rev. Lett. **70**, 2471 (1993).

[34] R. M. Feenstra and J. A. Stroscio, J. Vac. Sci. Technol. B **5**, 923 (1987).

[35] E. T. Yu, J. O. McCaldin, and T. C. McGill, Solid State Phys. **46**, 1 (1992).

[36] U. Seidel, B. E. Sagol, C. Pettenkofer, and T. Hannappel, Appl. Surf. Sci. **255**, 722 (2008).

[37] T. Sawada, K. Numata, S. Tohdoh, T. Saitoh, and H. Hasegawa, Jpn. J. Appl. Phys., Part 1 **32**, 511 (1993).

[38] H. H. Wieder, J. Vac. Sci. Technol. B **21**, 1915 (2003).

[39] L. F. J. Piper, T. D. Veal, M. J. Lowe, and C. F. McConville, Phys. Rev. B **73**, 195321 (2006).

[40] J. V. Laar, A. Huijser, and T. L. V. Rooy, J. Vac. Sci. Technol. **14**, 894 (1977).

[41] C. J. Chen, *Introduction to Scanning Tunneling Microscopy* (Oxford University Press, New York, 1993).

[42] R. M. Feenstra, G. Meyer, F. Moresco, and K. H. Rieder, Phys. Rev. B **66**, 165204 (2002).

[43] P. De Padova, C. Quaresima, P. Perfetti, R. Larciprete, R. Brochier, C. Richter, V. Ilakovac, P. Bencok, C. Teodorescu, V. Y. Aristov, R. L. Johnson, and K. Hricovini, Surf. Sci. **482–485**, 587 (2001).

[44] I. Aureli, V. Corradini, C. Mariani, E. Placidi, F. Arciprete, and A. Balzarotti, Surf. Sci. **576**, 123 (2005).

[45] M. C. Håkansson, L. S. O. Johansson, C. B. M. Andersson, U. O. Karlsson, L. O. Olsson, J. Kanski, L. Ilver, and P. O. Nilsson, Surf. Sci. **374**, 73 (1997).